

Using a multistate Mapping Approach to Surface Hopping to predict the Ultrafast Electron Diffraction signal of gas-phase cyclobutanone

Lewis Hutton,¹ Andrés Moreno Carrascosa,¹ Andrew W. Prentice,² Mats Simmermacher,¹ Johan E. Runeson,¹ Martin J. Paterson,² and Adam Kirrander¹

¹*Physical and Theoretical Chemistry Laboratory, Department of Chemistry, University of Oxford, Oxford OX1 3QZ, United Kingdom.*

²*Institute of Chemical Sciences, School of Engineering and Physical Sciences, Heriot-Watt University, Edinburgh EH14 4AS, United Kingdom.*

(*Electronic mail: adam.kirrander@chem.ox.ac.uk)

(*Electronic mail: lewis.hutton@chem.ox.ac.uk)

(Dated: 16 February 2024)

Using the recently developed multistate mapping approach to surface hopping (multistate MASH) method combined with SA(3)-CASSCF(12,12)/aug-cc-pVDZ electronic structure calculations, the gas-phase isotropic ultrafast electron diffraction (UED) of cyclobutanone is predicted and analyzed. After excitation into the n-3s Rydberg state (S_2), cyclobutanone can relax through two S_2/S_1 conical intersections, one characterized by compression of the CO bond, the other by dissociation of the α -CC bond. Subsequent transfer into the ground state (S_0) is then achieved via two additional S_1/S_0 conical intersections that lead to three reaction pathways: α ring-opening, ethene/ketene production, and CO liberation. The isotropic gas-phase UED signal is predicted from the multistate MASH simulations, allowing for a direct comparison to experimental data. This work, which is a contribution to the cyclobutanone prediction challenge, facilitates the identification of the main photoproducts in the UED signal and thereby emphasizes the importance of dynamics simulations for the interpretation of ultrafast experiments.

I. INTRODUCTION

The photochemistry of cyclic ketones has been studied extensively.^{1–6} Despite their small size, they have a rich photochemistry with multiple competing pathways that include dissociation, fluorescence, and intersystem crossing.^{7,8} The relative importance of the different pathways is closely linked to the size of the organic ring and the associated ring strain.⁷ The photodissociation of cyclic ketones has been of particular interest ever since the pioneering work of Norrish.⁹

A target of recurring interest in this class of molecules is cyclobutanone, $(\text{CH}_2)_3\text{CO}$.^{1,2,7,10–12} Early experimental studies identified the photoproducts of cyclobutanone as propylene (cyclopropane) and carbon monoxide ($\text{C}_3\text{H}_6 + \text{CO}$) or ethylene and ketene ($\text{CH}_2\text{CH}_2 + \text{CH}_2\text{CO}$). The corresponding quantum yields were found to be 40% and 60%,¹ although these quantum yields were later shown to have a strong dependence on the excitation wavelength.⁸ Recent experimental work includes ultrafast transient absorption spectroscopy on cyclobutanone in solution.⁷ Upon excitation to the S_1 ($n\pi^*$) state using UV pulses in the range 255–312 nm UV pulses, Kao *et al.* found that singlet dissociation pathways are dominant at shorter wavelengths, predominantly via Norrish Type-1 α cleavage, with minor contributions from ketene formation. At higher excitation energies, such as 200 nm, the n-3s Rydberg state comes into play.^{13–15} In this regime, using time-resolved mass spectrometry and photoelectron spectroscopy, Kuhlman *et al.* found that a ring puckering mode effectively couples the S_2 and S_1 states, allowing for rapid internal conversion.¹⁶

The experimental studies have been accompanied by theoretical work. Electronic structure calculations using complete active space self-consistent field, CASSCF(10,8), and mul-

tistate complete active space second-order perturbation theory, MS-CASPT2(10,8), predicted a small barrier for ring-opening on the S_1 state, with the possibility of minor contributions from barrierless dissociation in the T_1 state.¹⁷ Building on this, simulations of cyclobutanone by *ab initio* multiple spawning (AIMS) found a ring-opening mechanism to be dominant with a small portion of trajectories producing $\text{CH}_2=\text{CH}_2 + \text{CH}_2\text{CO}$ and $\text{CH}_2\text{CH}_2 + \text{CH}_2=\text{CO}$ fragmentation.¹⁸ We also note that Kuhlman *et al.* constructed a five-dimensional linear-vibronic Hamiltonian (LVH) model to simulate the S_2/S_1 decay in cyclobutanone using the multiconfigurational time-dependent Hartree (MCTDH) method, which succeeded in replicating the short time constants of 0.95 ps.¹⁹

The current paper is motivated the prediction challenge based on an UED experiment carried out at the SLAC MeV-UED facility.²⁰ Ultrafast electron diffraction has emerged as a powerful experimental technique for observing molecular dynamics in the recent decade,^{21–25} alongside ultrafast x-ray scattering.^{26–29} Notably, both techniques have made advances in extracting information that extends beyond structural dynamics.^{30,31} We use this challenge as an opportunity to benchmark the electronic structure calculations for cyclobutanone. This comparison includes non-standard selected-CI electronic structure methods that overcome the issue of large active space selection, constitute a black-box alternative to complete active space (CAS) methods and provide complementary benchmarks.^{32,33} The nonadiabatic simulations are carried out using the newly developed multistate MASH method.³⁴ Furthermore, we use the simulations to predict the UED signals and analyze these to determine the main contributions to the scattering.

II. THEORETICAL METHODS

A. Nonadiabatic Molecular dynamics

Many computational methods have been developed to simulate nonadiabatic dynamics over the past decades. Some, such as MCTDH^{35,36} and Multi-Layer MCTDH,³⁷ can provide numerically exact results. However, these methods require high-accuracy precomputed potential energy surfaces (PESs), which, combined with the exponential scaling of quantum mechanics, imposes severe limitations on the number of degrees of freedom that can be treated. To circumvent this problem, the nuclear wavefunction can be represented as a linear combination of traveling Gaussian basis functions or classically-guided trajectories, and the electronic structure quantities needed can be calculated *on-the-fly*, also known as direct dynamics. Such approaches can significantly reduce the phase space explored and therefore the computational cost per degree of freedom. *On-the-fly* methods include examples where the nuclei are propagated using equations of motion derived from the variational principle, notably variational multiconfigurational Gaussian (vMCG),^{38–40} or semiclassically, which includes methods such as full or *ab initio* multiple spawning (FMS/AIMS)^{41–44} and multiconfigurational Ehrenfest (MCE),^{45–47} or classically, such as trajectory surface hopping (TSH).⁴⁸ In addition to the above methods, mapping methods treat the electronic and nuclear degrees of freedom in an equal manner. Examples include the Meyer-Miller-Stock-Thoss (MMST) mapping Hamiltonian, symmetrical quasi-classical windowing, and generalized spin mapping.^{49–52} Ideas from this last category informed the development of the surface-hopping variant used in this paper (see Section II A 2 below). For an in-depth overview of different methods for nonadiabatic dynamics, the reader is directed towards the edited volume in reference 53.

1. Trajectory surface hopping

For nonadiabatic molecular dynamics, TSH is perhaps the most commonly employed approach to support the interpretation of experiments.^{54–61} In TSH, an ensemble of individual trajectories is used to represent the propagation of the nuclear wavepacket. In each trajectory, the nuclei are treated classically and the electronic amplitudes are used to predict hops to other electronic states. For a full discussion of TSH please see reference 62, while we continue by highlighting the key aspects of the fewest switches surface hopping (FSSH) variant of TSH.

Each trajectory in FSSH is initialized by projecting a ground-state vibrational distribution into the excited state of interest. We consider pure excitation, *i.e.* $c_a = 1$, where c_a is the electronic wavefunction coefficient for the active state a . The nuclear coordinates, $\bar{\mathbf{R}}$, are propagated using classical equations of motion,

$$\frac{d^2 \bar{\mathbf{R}}_\alpha}{dt^2} = -\frac{1}{M_\alpha} \nabla_\alpha E_a, \quad (1)$$

for each atom α , with t the time, M_α the mass of atom α , and $\nabla_\alpha E_a$ the gradient (force) on the *active* electronic adiabatic state. The integration is typically carried out using a standard velocity-Verlet scheme, though other propagators may be able to achieve better convergence.⁶³ The forces are normally obtained from electronic structure calculations of adiabatic states. In parallel with the nuclear propagation, one must integrate the electronic coefficients, $c = (c_1, \dots, c_N)$, for the N electronic states considered. In the adiabatic representation, the probability $P_{a \rightarrow b}^{\text{FSSH}}$ of a hop from state a to state b , is evaluated according to,

$$P_{a \rightarrow b}^{\text{FSSH}} = \max \left[0, \frac{2\Delta t}{|c_a|^2} \text{Re}(\mathbf{d}_{ab} \cdot \bar{\mathbf{v}} c_b c_a^*) \right], \quad (2)$$

where \mathbf{d}_{ab} is the nonadiabatic coupling vector between states a and b , $\bar{\mathbf{v}}$ is the classical nuclear velocity, c_a and c_b are the electronic coefficients for states a and b , and Δt is the timestep.⁶⁴ In some cases, an overlap scheme is employed to avoid the expensive calculations of nonadiabatic couplings.^{65,66} At each time step, $P_{a \rightarrow b}^{\text{FSSH}}$ is evaluated and compared to a random number, resulting in either acceptance or rejection of the hop. If a hop is accepted but the energy in the system is insufficient for it to occur, the hop is rejected and the nuclear velocities are reflected. This scenario is referred to as a frustrated hop. For hops that do take place, the active state is updated ($a \rightarrow b$), the velocities are modified to conserve total energy, and the trajectories continue to be propagated using the forces on the new active state.

The algorithm presented above is robust, but also causes one of the most well-known shortcomings of TSH, the so-called overcoherence issue. A number of, more or less *ad hoc*, decoherence correction schemes have been developed in response.^{67,68} The method presented next aims to alleviate the need for such *ad hoc* corrections.

2. Multistate mapping approach to surface hopping

Recently, a new version of TSH was devised by Manouch and Richardson, known as "mapping approach to surface hopping" (MASH).⁶⁹ MASH combines elements of mapping methods with TSH to attempt to get the advantages of both. Hence, in contrast to the stochastic algorithm in FSSH, MASH uses a deterministic algorithm to evaluate the active state,

$$P_{a \rightarrow b}^{\text{MASH}} = \begin{cases} 1, & \text{if } |c_b|^2 > |c_a|^2 \\ 0, & \text{otherwise.} \end{cases} \quad (3)$$

In other words, MASH defines the active state to be the state with the largest value of $|c_i|^2$, alleviating the need for *ad hoc* decoherence corrections and improving accuracy when compared to the original FSSH procedure.⁶⁹ Originally, MASH was formulated for two-state systems, but MASH was then generalized to any number of states by Runeson and Manolopoulos, giving rise to what we hereon refer to as multistate MASH.^{34,70}

To start trajectories, multistate MASH determines the nuclear initial conditions in the same manner as TSH, mapping the ground-state wavefunction onto a classical phase space. However, following other mapping approaches, MASH also considers the electronic coefficients c as a phase space variable. Therefore, rather than describing the initial state as pure, such as is done in FSSH, multistate MASH represents the initial state as a distribution over all values of $c = (c_1, \dots, c_N)$. In practice, this is done by random assignment of the complex-valued coefficients, $c_i = x_i + iy_i$, for each electronic state from Gaussian distributions with zero mean and standard deviation one for both the real and imaginary components. The resulting set of coefficients is normalized such that $1 = \sum_{i=1}^N |c_i|^2$. Coefficients where the initial state of interest does *not* have the largest absolute value are resampled until suitable sets are found. It is worth noting that other choices of initial distributions are possible, but have been found to yield similar results in most cases.³⁴ Therefore, we use this method of selecting initial conditions due to its ease of implementation.

To measure populations, several different estimators have been proposed in the literature. In this paper we measure the active state, corresponding to an estimator of the form

$$\Theta_n(t) = \begin{cases} 1, & \text{if } P_n(t) > P_m(t) \forall m \neq n \\ 0, & \text{otherwise} \end{cases} \quad (4)$$

With this choice of estimator and the initial distribution described above, the ensemble-averaged population transfer from state i to state n is

$$P_{i \rightarrow n}(t) = \langle \Theta_i(0) \Theta_n(t) \rangle \quad (5)$$

In the two-state case, Mannouch and Richardson have shown that this prescription overestimates the rate of transfer compared to Landau-Zener theory. It does, however, maintain a physical population estimate with a low number of trajectories. Note, that this approach is different from what is used in both MASH and multistate MASH. Other alternatives can be seen in the SI.

One potential side-effect of multistate MASH is hopping between states that are not coupled. It is possible to nevertheless accept all hops, regardless of the coupling between the states, which was the approach taken in reference 34. However, due to the risk of unphysical behavior, we introduce for all hops an energy criterion, such that $|E_a - E_b| < 0.055$ Hartree (≈ 1.5 eV) to prevent erroneous hops between uncoupled states. Hops that do not meet this criterion are treated on the same footing as reflected hops, with the total velocity of all atoms reflected. This direction of rescaling differs from previous work with MASH and is chosen due to simplicity.

B. Ultrafast electron diffraction (UED)

We simulate electron diffraction using the independent atom model (IAM), originally devised by Debye.^{71–74}

This method, extensively used in the analysis of scattering and crystallography experiments, approximates the electron scattering probability, $|Z(\mathbf{s}, \bar{\mathbf{R}})|^2$, as a coherent sum of tabulated⁷⁵ form factors, $f_N^e(\mathbf{s})$,

$$|Z(\mathbf{s}, \bar{\mathbf{R}})|^2 = \sum_A \sum_B^{N_{\text{at}}} f_A^e(\mathbf{s}) f_B^e(\mathbf{s}) e^{i\mathbf{s} \cdot \mathbf{R}_{AB}}, \quad (6)$$

where \mathbf{s} is the momentum transfer vector, $\bar{\mathbf{R}}$ the molecular geometry, \mathbf{R}_{AB} the distance vector between atoms A and B , and N_{at} the number of atoms in the molecule. Note that $|Z(\mathbf{s}, \bar{\mathbf{R}})|^2$ is given in units of the Rutherford cross-section (see *e.g.* reference 74 for further details). The electron scattering atomic form factors, $f_A^e(\mathbf{s})$, are defined as,

$$f_A^e(\mathbf{s}) = f_A^x(\mathbf{s}) - Z_A, \quad (7)$$

where $f_A^x(\mathbf{s})$ are the tabulated form factors for x-rays and Z_A the nuclear charges.

We calculate the rotationally averaged signal accounting for all possible molecular orientations in a thermal ensemble. This yields the isotropic elastic electron scattering probability, $\mathcal{S}_0(\mathbf{s}, \bar{\mathbf{R}})$, which takes the form,

$$\mathcal{S}_0(\mathbf{s}, \bar{\mathbf{R}}) = \sum_A \sum_B^{N_{\text{at}}} f_A^e(\mathbf{s}) f_B^e(\mathbf{s}) j_0(sR_{AB}), \quad (8)$$

where $s = |\mathbf{s}|$ is the norm of the momentum transfer vector and $R_{AB} = |\mathbf{R}_{AB}|$ is the distance between atoms A and B , and where we have introduced the zeroth-order spherical Bessel function $j_0(sR_{AB})$ defined as,

$$j_0(sR_{AB}) = \frac{\sin(sR_{AB})}{sR_{AB}}. \quad (9)$$

In the experiment, not only the elastic component of electron scattering is measured but also the inelastic component. While the IAM cannot describe individual inelastic transitions, the total inelastic component can be approximated by an incoherent sum of *atomic* inelastic scattering functions $S_A(s)$. This yields the total isotropic scattering, $\mathcal{S}_I(\mathbf{s}, \bar{\mathbf{R}})$, as the sum of the elastic and inelastic contributions,

$$\mathcal{S}_I(\mathbf{s}, \bar{\mathbf{R}}) = \mathcal{S}_0(\mathbf{s}, \bar{\mathbf{R}}) + \sum_A^{N_{\text{at}}} S_A(s). \quad (10)$$

We note that further improvements in the scattering signal are straightforward. For instance, alignment effects resulting from the linear polarization of the pump laser can be accounted for⁷⁶ and corrections to the form factors due to relativistic effects can be made,⁷⁷ however for the latter we note that this effect is comparatively minor for the electron energies at the SLAC MeV-UED source. It is also possible to calculate the scattering cross-sections from *ab initio* electronic wavefunctions, which makes it possible to account accurately for the effects on scattering from chemical bonding, electron correlation, and change in the electronic state due to excitation by the pump pulse.^{78–80}

III. COMPUTATIONAL DETAILS

A ground-state minimum energy structure of cyclobutanone was obtained using state-averaged CASSCF,⁸¹ SA(3)-CASSCF(12,12)/aug-cc-pVDZ, *i.e.* state-averaging over the three lowest singlet states, an active space with 12 electrons in 12 orbitals with the aug-cc-pVDZ Cartesian basis.⁸² Further details are given in the supplementary information. All electronic structure calculations were done in OpenMolcas version v23.02-10-gb7266214b.^{83,84} The ground-state minimum energy structure was subjected to a frequency calculation yielding no imaginary frequencies, confirming the structure to be a true minimum. Further excited state structures were optimized using SA(3)-CASSCF(12,12) to obtain the S_2 minimum, two S_2/S_1 minimum energy conical intersections (MECIs), and two S_1/S_0 MECIs. Selected structures were subjected to linear interpolation in internal coordinates (LIIC) to yield a progression of intermediate structures. Potential energy curves along the LIICs were calculated using SA(3)-CASSCF(12,12) and extended multistate complete active space second-order perturbation theory, XMS-CASPT2, with the same (12,12) active space as for the CASSCF calculations (see supplementary information).⁸⁵ For stability, an imaginary shift of 0.5 a.u. was applied for all XMS-CASPT2 calculations.⁸⁶

For further comparison, the potential energy curves were also calculated using a modified version of adaptive configuration interaction (ACI) and Monte-Carlo configuration interaction (MCCI).⁸⁷⁻⁸⁹ The state-averaged MCCI calculations were performed using MCCI V4^{90,91} with the SA error-controlled calculations performed using a locally modified development version of GeneralSCI 1.0.⁹² Further details are given in the supplementary information.

The calculated ground state frequencies were used to generate a Wigner distribution from which 1000 geometries were sampled. At each geometry, excitation energies and oscillator strengths were calculated using SA(3)-CASSCF(12,12). The photoabsorption cross-section was constructed using the nuclear ensemble approach (NEA), convoluted by Lorentzian functions with a phenomenological broadening parameter of 0.05 eV.⁹³ Initial conditions for the multistate MASH were sampled from this Wigner distribution using an implicit laser pulse of width 0.2 eV, centered at 6.2 eV. All trajectories were initiated from the bright S_2 (n-3s Rydberg) state using multistate MASH (see section II A 2 for more details)³⁴ implemented in a development version of SHARC.⁹⁴ The electronic structure calculations were carried out using SA(3)-CASSCF(12,12)/aug-cc-pVDZ with all three electronic states available in dynamics. The trajectories were propagated using a 0.5 fs time step, with 25 substeps, for 300 fs using a local diabaticization scheme. For trajectories in which the total energy changes by more than 0.25 eV, the propagation is stopped and only the time points with the correct total energy are used in the analysis. Additionally, we note that a subset of trajectories are 'trapped'. This occurs when the trajectories enter a region where a reflected hop happens but the reflected hop fails to remove the trajectory from the 'forbidden' region. Such trapped trajectories are only included in the analysis until the

TABLE I. Table of excitation energies in eV for the lowest two excited electronic states of cyclobutanone at the S_0 minimum energy geometry optimized using SA(3)-CASSCF(12,12)/aug-cc-pVDZ. State characters are given in parentheses along with excitation energies.

Method	S_1	S_2
SA(3)-CASSCF(12,12)	4.44 ($n\pi^*$)	6.24 (n-3s)
XMS-CASPT2(12,12)	4.40 ($n\pi^*$)	6.20 (n-3s)
SA(3)-ACI	4.43 ($n\pi^*$)	6.31 (n-3s)
SA(3)-MCCI	4.45 ($n\pi^*$)	6.30 (n-3s)

point that they get trapped. For a summary of the trajectories removed from the analysis, see the supplementary information. Populations of the ensemble of trajectories are estimated using the multistate Populations were estimated according to Section II A 2. Finally, rotationally averaged total scattering diffraction patterns were calculated using the geometries from the multistate MASH trajectories and the independent atom model (see Section II B) for the initial 200 fs of dynamics.

IV. RESULTS AND DISCUSSION

A. Excited states of cyclobutanone

The character of the two lowest-lying S_1 and S_2 electronic states of cyclobutanone has previously been identified as $n\pi^*$ and n-3s, respectively.^{13,16} The next set of excited states are the higher-lying 3p Rydberg states, which appear a full 0.7 eV above the n-3s Rydberg state.¹⁴ Triplet states have been shown to be important for the photodynamics upon excitation with long wavelengths.⁷ However, due to the short excited state lifetime of cyclobutanone following excitation into the S_2 state, triplet states are less likely to make a significant contribution to the current photodynamics. For these reasons, we have chosen to focus our attention on an accurate description of the two lowest-lying singlet states S_1 and S_2 .

A summary of the low-lying excited singlet states available to cyclobutanone at the equilibrium geometry of cyclobutanone is shown in Table I. Both SA(3)-CASSCF(12,12) and XMS-CASPT2(12,12) yield an S_1 state with $n\pi^*$ character at the Franck-Condon (FC) geometry and an S_2 state with n-3s Rydberg character. Furthermore, the excitation energies for SA(3)-CASSCF(12,12) are in excellent agreement with XMS-CASPT2(12,12), with SA(3)-CASSCF(12,12) energies showing a constant difference of 0.04 eV for both excited states. Excitation energies for SA(3)-ACI and SA(3)-MCCI can also be found in Table I. These methods give a good description of the low-lying singlet states of cyclobutanone with excitation energies deviating by ~ 0.05 eV for the valence $n\pi^*$ state and ~ 0.1 eV for the n-3s Rydberg state compared to the XMS-CASPT2(12,12) benchmark. In the ACI simulation, a large orbital window, corresponding to a CAS-CI(12,36), has also been tested. The large orbital window gives results analogous to the ones obtained with CASSCF(12,12), providing further support for this choice of active space.

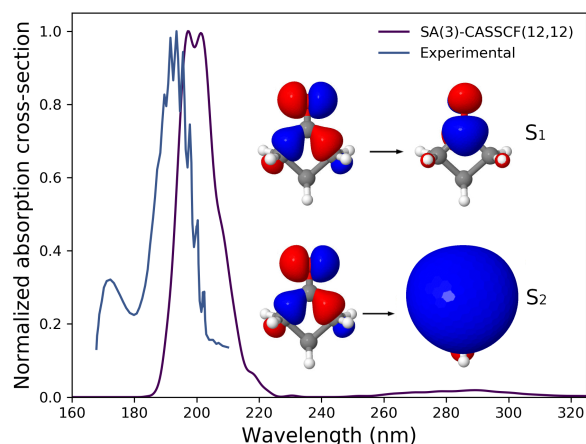


FIG. 1. Photoabsorption cross-section of gas-phase cyclobutanone calculated using the SA(3)-CASSCF(12,12)/aug-cc-pVDZ, the NEA and Wigner sampling of 1000 geometries (purple line). Experimental data is reproduced from reference 95 (blue line). Orbitals for the S_1 and S_2 states are shown as an inset.

A theoretical photoabsorption cross-section of cyclobutanone calculated using SA(3)-CASSCF(12,12) is shown in Fig. 1, allowing for a direct comparison with experimental absorption spectra. Good agreement can be observed between the two spectra, further validating our electronic structure method along with confirming the assignment of states using the insets in Fig. 1.

B. Photochemical reaction pathways and benchmarking

After the photophysics of cyclobutanone has been studied in the FC region, the different deactivation pathways available upon photoexcitation can be characterized. A series of potentially important optimized geometries for these pathways are shown in Fig. 2, optimized using SA(3)-CASSCF(12,12)/aug-cc-pVDZ. The S_0 minimum energy geometry (S_0 , upper left) can be characterized by a single carbon atom breaking the planar symmetry of the molecule, along with a C=O bond length of 1.19 Å and an α -CC bond of 1.58 Å. When the molecule is excited by a 200 nm pulse, the S_2 excited electronic state is populated at the FC region and can potentially relax into the S_2 minimum. The S_2 minimum energy geometry (S_2 , upper center) displays subtle changes in bond lengths, along with a planarization of the carbon ring. Two S_2/S_1 minimum energy conical intersections (MECIs) were successfully optimized, with the S_2/S_1 MECI (S_2/S_1 , lower left) already reported previously.¹⁹ This MECI displays a rather severe compression of the C=O bond. The second S_2/S_1 MECI (S_2/S_1 , upper right) exhibits a dissociated α -CC bond alongside a compressed C=O bond. Two further MECIs are included in Fig. 2, corresponding to MECIs between the ground and first excited state. Both these S_1/S_0 MECIs have been reported previously by Liu *et al.*¹⁸ The first of these MECIs (S_1/S_0 ,

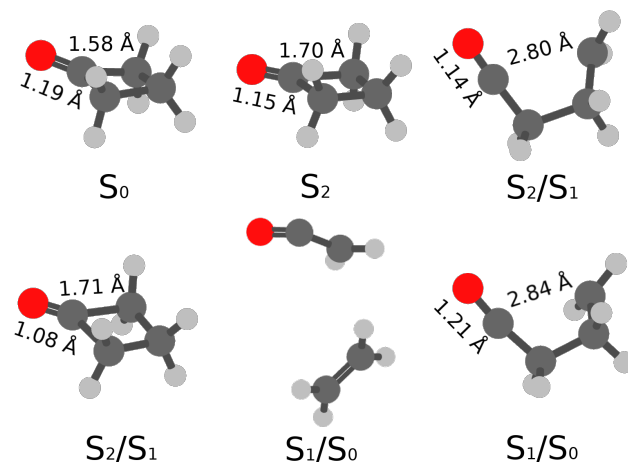


FIG. 2. Six critical geometries are shown for gas-phase cyclobutanone. The S_0 minimum (upper left), S_2 minimum (upper center), a dissociative S_2/S_1 MECI (upper right), another S_2/S_1 MECI (lower left), a ring breaking S_1/S_0 MECI (lower center), and a ring-opening S_1/S_0 (lower right). All structures shown are optimized using SA(3)-CASSCF(12,12)/aug-cc-pVDZ.

lower center), termed CI-3 in reference 18, breaks the ring structure to produce $\text{CH}_2=\text{CH}_2$ and $\text{O}=\text{CCH}_2$. The second S_1/S_0 MECI (S_1/S_0 , lower right), termed CI-1 in reference 18, is closely related to the second S_2/S_1 MECI (S_2/S_1 , upper right), with an dissociated α -CC bond. However, in contrast to the S_2/S_1 MECI, the S_1/S_0 MECI contains a slightly stretched C=O bond relative to the S_0 geometry. It is obvious from this static perspective of excited state geometries, that cyclobutanone possesses a rich photochemistry. However, the relative importance of each of these structures is still unknown, as are the final products of each conical intersection (CI).

To gain a better understanding of the PESs of cyclobutanone and to benchmark SA(3)-CASSCF(12,12) away from the FC region, an LIIC was done on some of the key geometries shown in Fig. 2. Four structures were selected: the S_0 minimum (Fig. 2, S_0 , upper left), S_2 minimum (Fig. 2, S_2 , upper center), the dissociative S_2/S_1 MECI (Fig. 2, S_2/S_1 , upper right) and finally the α -CC bond dissociation S_1/S_0 MECI (Fig. 2, S_1/S_0 , upper right).

Upon photoexcitation to the S_2 state, cyclobutanone in the S_0 minimum structure can relax to the closeby S_2 minimum via a planarization of the carbon ring (see green line in panel 1 of Fig. 3). Here, cyclobutanone undergoes a dissociation of an α -CC bond resulting in a barrier height of 0.21 eV for SA(3)-CASSCF(12,12), somewhat below the 0.49 eV predicted by XMS-CASPT(12,12), with the barrier heights given as energy differences relative the S_2 minimum. Note that absolute values for transition state barriers in LIICs should be treated with care as they are known to be overestimated. Regardless, SA(3)-CASSCF(12,12) is likely to estimate a faster rate of decay from S_2 to S_1 as a result of this smaller reaction barrier. A steep drop in energy is observed for both methods after the transition barrier leading down to the S_2/S_1 MECI (see Fig. 2,

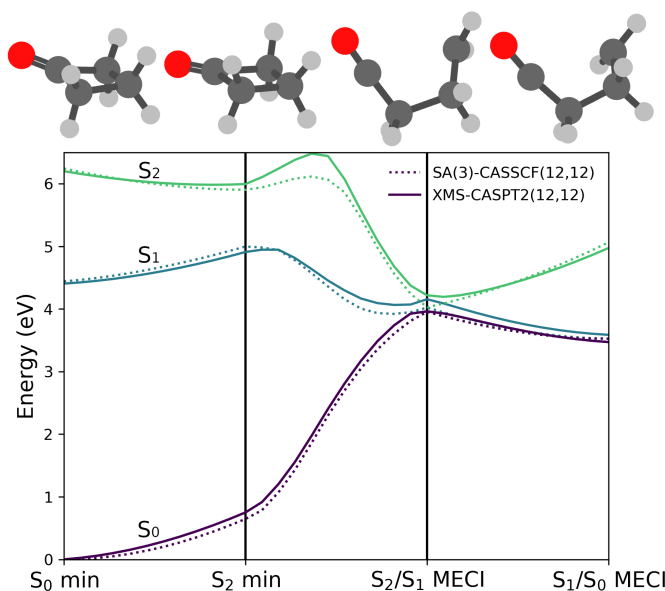


FIG. 3. A linear interpolation in internal coordinates from the S_0 minimum to S_2 minimum to the dissociative S_2/S_1 MECI ending with the ring opening S_1/S_0 MECI. Inset structures correspond to the optimized structures used along the LIIC coordinate. Excitation energies for the three lowest-lying singlet states are given using both SA(3)-CASSCF(12,12)/aug-cc-pVDZ (dotted line) and XMS-CASPT2(12,12)/aug-cc-pVDZ (solid line).

upper right and inset of Fig. 3). This S_2/S_1 MECI is peaked and has a single pathway according to the criteria set out in reference 96. This allows for efficient funneling onto the S_1 state (see blue line in Fig. 3) where a barrier-less decay is observed to the structurally similar S_1/S_0 MECI (see Fig. 2) where the S_1/S_0 MECI is observed with a peaked bifurcating branching space.

From Fig. 3 it can be deduced that there is excellent agreement between SA(3)-CASSCF(12,12) and XMS-CASPT2(12,12), with slight differences observed for the approximate transition barrier height. Nevertheless, overall the SA(3)-CASSCF(12,12) results offer an excellent compromise between speed and accuracy for the *on-the-fly* nonadiabatic dynamics of gas-phase cyclobutanone. Additional LIICs for the same geometries can be found in SI (Figures 3 and 4) for both SA(3)-ACI and SA(3)-MCCI. These further support our assessment. We also note that this indicates that good agreement can be obtained with methods that potentially offer a more black-box approach to the calculation of multireference wavefunctions than the CAS family of methods.

C. Dynamics

A total of 229 trajectories were initiated on the S_2 state. Trajectories were removed from the statistics if either a change in total energy of 0.25 eV or more was observed or if consecutive reflected hops indicated that the trajectory was

trapped in a 'forbidden' region of the PES. This resulted in a significant number of discarded trajectories. For a full summary of discarded trajectories see the SI (Figure 2). To briefly summarize, after 50 fs the number of trajectories had dropped to 146, and by 200 fs only 18 trajectories of the initial 229 trajectories had survived, while at 300 fs this was down to 10 trajectories. At 300 fs a total of 71 trajectories had been discarded due to consecutive reflected hops, while 148 trajectories had been discarded due to issues with the energy conservation. We acknowledge that this could potentially cause artifacts in the simulations, especially if certain processes are systematically removed or enhanced by the removal of trajectories.

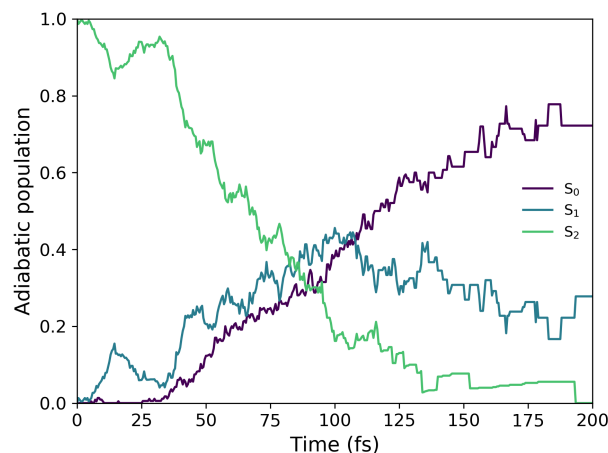


FIG. 4. Adiabatic populations for the three lowest-lying singlet states, S_{0-2} , given by the multistate MASH population estimator (Section II A 2) given as a function of time and taking all trajectories into account.

The adiabatic populations for the three electronic states S_{0-2} used in our simulations are given in Fig. 4 for the initial 200 fs of the dynamics. A rapid decay of the S_2 state (green line) can be observed after ~ 8 fs. This decay is correlated with a population increase on S_1 (teal line), indicating that fast initial dynamics on S_2 rapidly reaches an S_2/S_1 CI. For the early time dynamics ($t < 30$ fs), the ground-state can be seen to be inaccessible from the S_2 state (see panel 1 in Fig. 3). After 30 fs, there is a steady increase in the ground-state S_0 (purple line) population, showing passage through the S_1/S_0 CI and therefore formation of the photoproducts linked to each CI (Fig. 2). After 100 fs, we observe a decreased rate of population transfer from S_2 to S_1 , resulting in depletion of S_1 and an overall decrease in the population of the two excited states matched by the continued increase in the population of the ground state. After ~ 175 fs, the population transfer is largely over, although errors in this region will be high due to the small number of trajectories. The populations observed in Fig. 4 indicate ultrafast non-radiative deactivation pathways for cyclobutanone, there is then likely the possibility of further non-equilibrium ground-state chemistry as a result of very hot molecules in the ground state following the decay dynamics.

As shown previously, the deactivation pathways available to cyclobutanone imply the cleavage of one or two bonds in the ring structure. To identify these different pathways, the bond lengths for all multistate MASH trajectories are plotted, separated into α and β -CC bonds according to the inset in Fig. 5. Four distinct outcomes are observed:

- (i) There is no bond breaking (purple), and the molecule remains in the FC region. These are characterized by short α and β -CC bond lengths ($R < 2.2$ Å). It is important to note that the trajectories included in this group do not progress over 90 fs.
- (ii) There exists a single α -CC bond breaking (teal). This pathway gives rise to a ring-opened structure *i.e.* CH₂CH₂CH₂CO. This is indicated by an elongation of an α -CC bond, but due to the carbon backbone still being intact, the distance between the two carbon atoms is limited to $R \sim 4.5$ Å. This pathway is a result of passing through the S₁/S₀ CI (upper right in Fig. 2).
- (iii) Two α -CC bonds break to liberate CO, where there is a large increase in α -CC bonds to values above 4.5 Å (blue). Attempts to optimize an MECI using SA(3)-CASSCF(12,12) involving CO dissociation were unsuccessful, however, trajectories were observed with CO dissociation after having decayed to the ground state via the α -CC dissociation S₁/S₀ CI (lower right, Fig. 2). This means the CO dissociation takes place on the ground state rapidly after passing through a CI. It is worth noting for option *iii*) a single trajectory also displays ground state dissociation of CH₂CH₂CH₂ into CH₂CH₂ and CH₂, which can be seen in Fig. 5 as a blue line displaying increases in both α and β -CC bonds.
- (iv) An α -CC bond and β -CC bond breaking (pale green) showing the stepwise ring-breaking mechanism where ethene and ketene are produced. Here, an α -CC bond breaks first, followed by a β -CC bond breaking. This can be linked to the S₁/S₀ MECI in Fig. 2 (S₁/S₀, lower center).

D. UED

The nonadiabatic dynamics of cyclobutanone presented in the previous section has served as the basis for calculating the rotationally averaged total electron scattering signal as a function of time, using the independent atom model (IAM) as described in the theory section. To correctly account for the time evolution of the molecular geometries we use a percent difference in the form,

$$\%S_t(s,t) = 100 \times \frac{S_t(s,t) - S_t(s,0)}{S_t(s,0)}, \quad (11)$$

where $S_t(s,t)$ is the total electron scattering probability at time t and $S_t(s,0)$ is the total electron scattering probability at $t = 0$

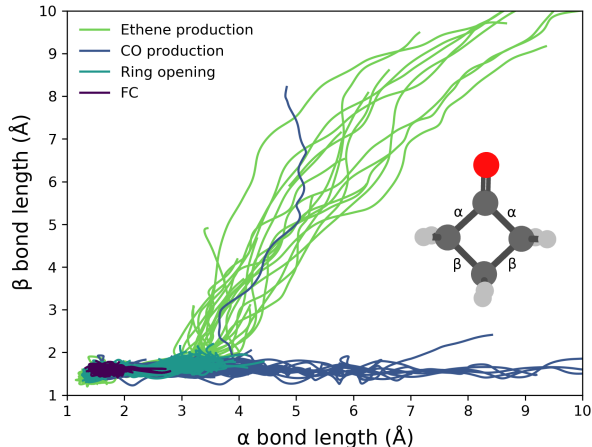


FIG. 5. A 2D projection of all CC bond lengths across all trajectories. The CC bonds are partitioned according to the labeling on the inset. Each trajectory is clustered based on the final geometry of the trajectory, resulting in four channels: *i*) FC, *ii*) ring opening, *iii*) CO production and *iv*) ethene production. See the main text for more details.

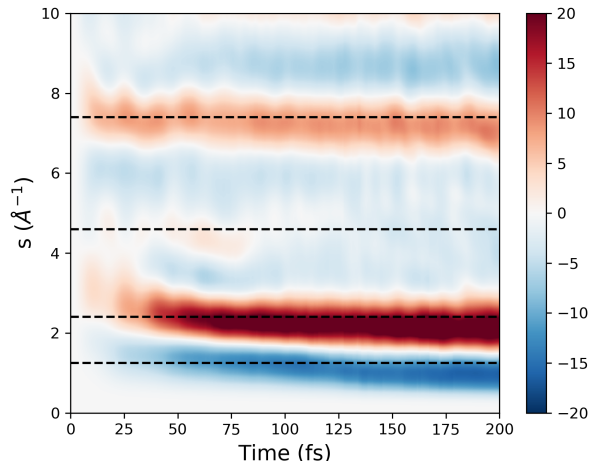


FIG. 6. Gas-phase UED pattern shown with percent difference as a function of time for cyclobutanone. All active trajectories are taken into account via the process described in section III. Dashed horizontal lines represent the key features of the UED pattern.

(*i.e.* before the pump). In Fig. 6, the time-resolved UED pattern for cyclobutanone is shown as a function of the amplitude of the momentum transfer vector s . Due to the rapid loss of trajectories during the simulations, discussed earlier, we only show the UED signal for the first 200 fs.

UED cross-section percent differences shown in Fig. 6 present four distinct features at $s \approx 1.25, 2.4, 4.6,$ and 7.4 Å⁻¹. These features constitute a fingerprint of the structural dynamics taking place in cyclobutanone, therefore, they can be interpreted with the help of additional static signals for the key geometries discussed in Sections IV B (purple line

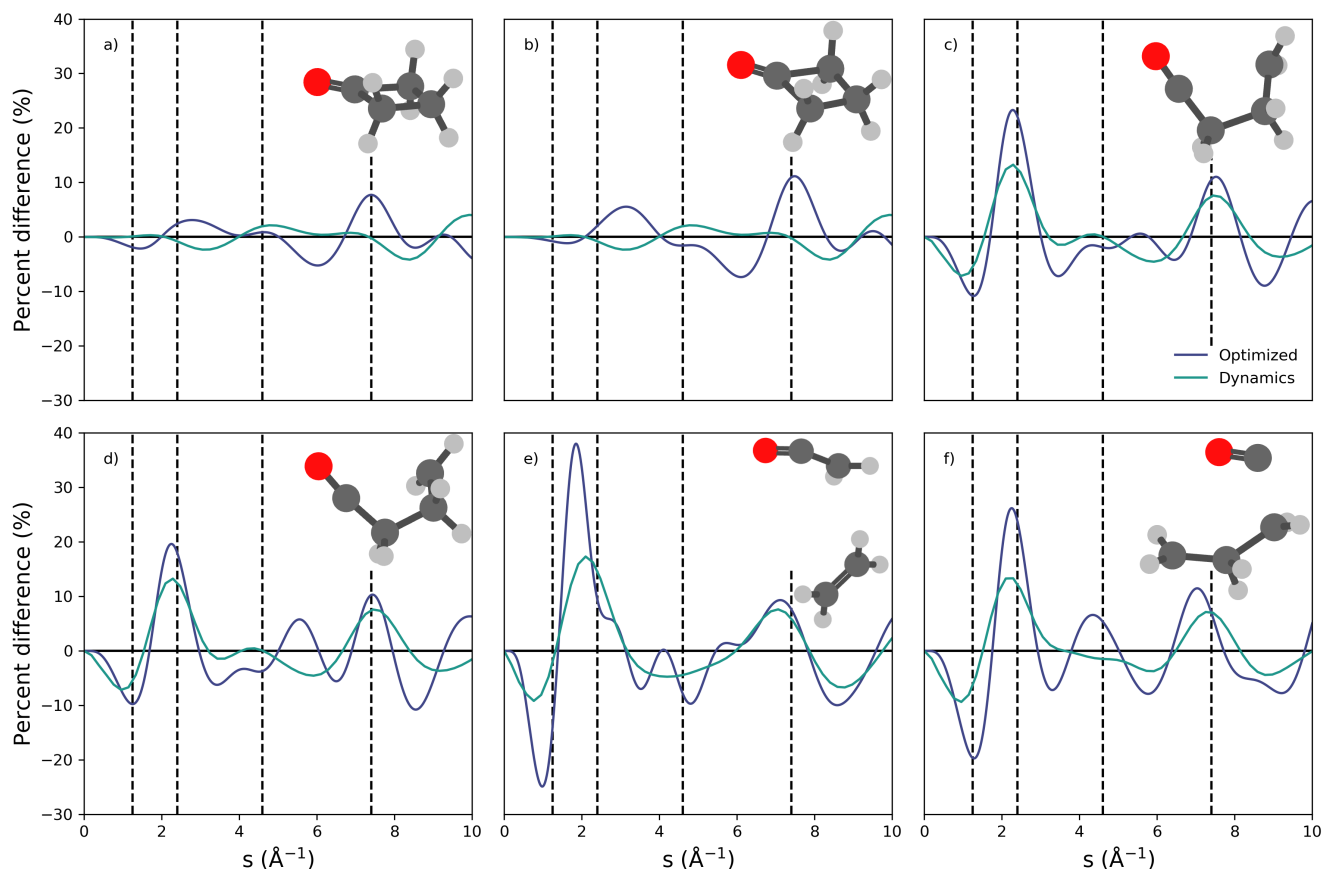


FIG. 7. Six static UED percent difference signals for key optimized geometries of gas-phase cyclobutanone and the static signal from an example structure obtained from our dynamics simulations showing CO dissociation (blue) and an average of the trajectories where the considered structure is the final product (green). Insets show the structure used to calculate the static signal: a) S_2 minimum, b) S_2/S_1 compression, c) S_2/S_1 α cleavage, d) S_1/S_0 α cleavage, e) S_2/S_1 ethene production and finally f) CO production. Vertical dashed lines match the horizontal dashed lines shown in Figure 6, showing key features in the overall UED.

in Fig. 7). A static signal for a fixed time (80 fs for panels a and b, and 150 fs for panels c and f) is also shown in Fig. 7 for each pathway (green lines), showing some broadening of the peaks due to vibrational dispersion, along with subtle shifts of peak maxima. In addition, the electron scattering cross-sections are calculated for the four individual outcomes using groups of trajectories in the dynamics simulation (*i,ii,iii,iv* in Section IV B) and shown in Fig. 8, to aid the interpretation of the results. Due to the significant similarities between the photoproducts and the high degree of symmetry in cyclobutanone, there is a large number of overlapping features in all static and individual cluster signals (see Figures 7 and 8). Based on these similarities, we postulate that the strong negative signal at $\sim 1.25 \text{ \AA}^{-1}$ and the strong positive feature at $\sim 2.4 \text{ \AA}^{-1}$, common to all possible photoproducts, are related to the breaking of one or two α -bonds to produce open-ring (*i*), CO and $\text{CH}_2\text{CH}_2\text{CH}_2$ (*ii*), or ethene and ketene (*iii*). These two features, which reach a maximum at $t \sim 50$ fs, are then related to the electronic state population transferring through the S_2/S_1 CI and subsequently through the S_1/S_0 CI (see Figures 7d), 7e) and 7f)). This timescale is consis-

tent with what is observed in the populations of S_1 and the S_0 ground state as shown in Fig. 4, but significantly faster than that observed in reference 19. It is possible that our simulations underestimate the time in S_2 due to a smaller barrier, as discussed in the context of Fig. 3 for SA(3)-CASSCF(12,12) compared to the matching XMS-CASPT2, resulting in somewhat fast decay and product formation.

The other UED feature common to the total signal (Fig. 6) and all individual pathways (Fig. 8) is an oscillatory positive signal at $s \approx 7.4 \text{ \AA}^{-1}$. For the initial 50 fs of simulation, in this s region, one can see strong coherent motions with an oscillatory period of ~ 15 fs, indicating a possible coherent vibrational motion. All bonds between heavy atoms (C and O) are plotted for an exemplary trajectory in the SI (Fig. 6). Only the CO bond length has a period that matches these oscillations, suggesting the carbonyl stretch may be responsible for this feature.

An additional feature can be observed at $s \sim 4.6 \text{ \AA}^{-1}$ with weak positive intensity for the initial 80 fs of the time-resolved UED, becoming weakly negative after. This positive weak feature (4–6 %) only shows in those pathways where β -bond

breaking does not occur (Figures 8a) and 8c)) and it is negative in the one where this happens (Fig. 8b)). When looking at the static signals in Fig. 7, one can see that the CO dissociation channel (Fig. 7f)) yields a positive signal at $s \sim 4.6 \text{ \AA}^{-1}$, and that this feature is also present in the ring-open structures (Fig. 7c) and 7d)) at $s \sim 4.9 \text{ \AA}^{-1}$. Therefore, one can relate the sign and strength of this feature to the separation between the two carbons forming the β bonds in the molecule (see inset in Fig. 5). The change of sign for this feature at $t \approx 80 \text{ fs}$, together with the great influence path *iv*) has on the dynamics, suggests the ethene and ketene formation can be directly observed by looking at this region of the time-resolved UED signal.

It is important to note that the FC group presents oscillatory behavior in all of the aforementioned UED features. These oscillations can be explained by taking into account that the molecule is vibrationally excited (*i.e.* hot) when the FC region is accessed, giving rise to high-amplitude motions. This behavior is not seen in the averaged signal due to the small contribution of this feature to the overall dynamics.

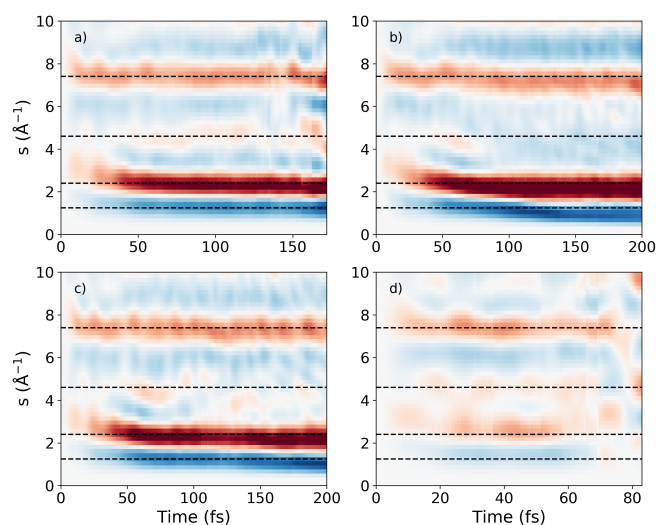


FIG. 8. Percent difference UED patterns for each cluster of trajectories reported in Fig. 5. Subplots show the clustered UED for: a) α -CC cleavage, b) ethene production, c) CO production, and d) FC. Clusters that do not contain data until the target 200 fs endpoint are truncated at the final data point.

V. CONCLUSIONS

In summary, motivated by an experiment at the SLAC MeV-UED facility and the associated prediction challenge, we have applied multistate MASH and SA(3)-CASSCF(12,12)/aug-cc-pVDZ to identify the gas-phase photodynamics of cyclobutanone after photoexcitation by 200 nm pump pulses into the n -3s Rydberg state. Mechanistic details have been identified using both a static analysis and nonadiabatic dynamics, finding a fast decay from the S_2 state into the S_1 via two CIs. A further two CIs allow for similarly fast access to the ground state. This results in the same set of photoproducts previously

observed, namely α ring-opening and ethene+ketene production, the former of which can further dissociate on the ground electronic state to liberate CO.

For direct comparison with experimental results we have also predicted the gas-phase isotropic UED signal of cyclobutanone (see Fig. 6). We find that there is significant overlap between several of the products meaning that the UED signal contains multiple features. However, several distinct features indicate the formation of reaction products and loss of cyclobutanone in the equilibrium geometry. The timescale of the reaction can also be inferred from the UED signals, which, unsurprisingly, closely matches that of our simulated reaction dynamics. However, we do note that the reaction, in our simulations, proceeds significantly faster than previous observations.^{16,19}

Significant caveats remain for our predictions. The instability of the active space means that we could be potentially blind to certain reaction channels. Additionally, the value obtained for each channel's quantum yield is susceptible to significant errors from the choice of electronic structure method and the associated instabilities. This does highlight the need for robust 'black-box' electronic structure methods compatible with *on-the-fly* nonadiabatic dynamics simulations. Methods such as ADC(2) or TDDFT already exist, but are not universally applicable as they have well-documented flaws. A potential way forward, could be the selected CI family of methods,^{90,91} some benchmarking of which has been already been included in our results. Further development and benchmarking of these methods is required to confirm whether they indeed offer accurate electronic structure in a more robust, black-box fashion. Also, it is important to add that the truncation of trajectories due to uncoupled hops affects the statistics of the dynamics, and therefore needs to be refined in future work. Finally, the multistate MASH used in the simulations is still being developed, and we anticipate that refinement of the algorithm will improve the results further.

VI. ACKNOWLEDGEMENTS

The authors would like to thank the organizers of the cyclobutanone prediction challenge for arranging this special edition. AK, MJP, LH, and AP acknowledge funding from the Leverhulme Trust (RPG-2020-208), and AK, AMC and MJP further acknowledge EPSRC EP/V006819. AK also acknowledges EPSRC EP/V049240 and grant DE-SC0020276 from the US Department of Energy. JER was funded by a mobility fellowship from the Swiss National Science Foundation under Award P500PN_206641/1.

¹S. W. Benson and G. B. Kistiakowsky, "The Photochemical Decomposition of Cyclic Ketones," *Journal of the American Chemical Society* **64**, 80–86 (1942).

²E. K. C. Lee, R. G. Shortridge, and C. F. Rusbult, "Fluorescence excitation study of cyclobutanone, cyclopentanone, and cyclohexanone in the gas phase," *Journal of the American Chemical Society* **93**, 1863–1867 (1971).

³M. Baba and I. Hanazaki, "The $S_1(n, \pi^*)$ states of cyclopentanone and cyclobutanone in a supersonic nozzle beam," *The Journal of Chemical Physics* **81**, 5426–5433 (1984).

- ⁴K. Y. Tang and E. K. C. Lee, "Laser photolysis of cyclobutanone. Photodecomposition from selected vibronic levels at long wavelengths," *The Journal of Physical Chemistry* **80**, 1833–1836 (1976).
- ⁵R. Harrison, H. Hawkins, R. Leo, and P. John, "The absorption of pulsed infrared radiation by cyclobutanone and its subsequent decomposition," *Chemical Physics Letters* **70**, 555–559 (1980).
- ⁶G. C. Causley and B. R. Russell, "Electric dichroism spectroscopy in the vacuum ultraviolet. I. Cyclobutanone, cyclopentanone, cyclohexanone, and cycloheptanone," *The Journal of Chemical Physics* **72**, 2623–2631 (1980).
- ⁷M. H. Kao, R. K. Venkatraman, M. N. Ashfold, and A. J. Orr-Ewing, "Effects of ring-strain on the ultrafast photochemistry of cyclic ketones," *Chemical Science* **11**, 1991–2000 (2020).
- ⁸J. C. Hemminger and E. K. C. Lee, "Fluorescence Excitation and Photodecomposition of the First Excited Singlet Cyclobutanone (1A₂): A Study of Predissociation of and Collisional Energy Transfer from the Vibronically Selected Species," *The Journal of Chemical Physics* **56**, 5284–5295 (1972).
- ⁹O. D. Saltmarsh and R. G. W. Norrish, "Primary photochemical reactions. Part VI. The photochemical decomposition of certain cyclic ketones," *Journal of the Chemical Society*, 455–459 (1935).
- ¹⁰H. O. Denschlag and E. K. C. Lee, "Benzene photosensitization and direct photolysis of cyclobutanone and cyclobutanone-2-t in the gas phase," *Journal of the American Chemical Society* **90**, 3628–3638 (1968).
- ¹¹N. E. Lee and E. K. C. Lee, "Tracer Study of Photochemically Excited Cyclobutanone-2- t and Cyclobutanone. II. Detailed Mechanism, Energetics, Unimolecular Decomposition Rates, and Intermolecular Vibrational Energy Transfer," *The Journal of Chemical Physics* **50**, 2094–2107 (1969).
- ¹²E. W. Diau, G. Kötting, and A. H. Zewail, "Femtochemistry of norrish type-1 reactions: ii. the anomalous predissociation dynamics of cyclobutanone on the S₁ surface," *ChemPhysChem* **2**, 294–309 (2001).
- ¹³C. R. Drury-Lessard and D. C. Moule, "Ring puckering in the 1B₂ (n, 3s) Rydberg electronic state of cyclobutanone," *The Journal of Chemical Physics* **68**, 5392–5395 (1978).
- ¹⁴L. O'Toole, P. Brint, C. Kosmidis, G. Boulakis, and P. Tsekeris, "Vacuum-ultraviolet absorption spectra of propanone, butanone and the cyclic ketones C_nH_{2n-2}O (n = 4, 5, 6, 7)," *J. Chem. Soc., Faraday Trans.* **87**, 3343–3351 (1991).
- ¹⁵R. F. Whitlock and A. B. Duncan, "Electronic spectrum of cyclobutanone," *The Journal of Chemical Physics* **55**, 218–224 (1971).
- ¹⁶T. S. Kuhlman, T. I. Sølling, and K. B. Møller, "Coherent Motion Reveals Non-Ergodic Nature of Internal Conversion between Excited States," *ChemPhysChem* **13**, 820–827 (2012).
- ¹⁷S. H. Xia, X. Y. Liu, Q. Fang, and G. Cui, "Excited-state ring-opening mechanism of cyclic ketones: A MS-CASPT2//CASSCF study," *Journal of Physical Chemistry A* **119**, 3569–3576 (2015).
- ¹⁸L. Liu and W. H. Fang, "New insights into photodissociation dynamics of cyclobutanone from the AIMS dynamic simulation," *Journal of Chemical Physics* **144** (2016), 10.1063/1.4945782.
- ¹⁹T. S. Kuhlman, S. P. A. Sauer, T. I. Sølling, and K. B. Møller, "Symmetry, vibrational energy redistribution and vibronic coupling: The internal conversion processes of cycloketones," *The Journal of Chemical Physics* **137** (2012), 10.1063/1.4742313.
- ²⁰T. J. Martínez, T. Wolf, Slavíček, G. Worth, M. Barbatti, B. Curchod, and S. Bonella, "Prediction Challenge: Cyclobutanone Photochemistry," <https://publishing.aip.org/publications/journals/special-topics/jcp/prediction-challenge-cyclobutanone-photochemistry/> accessed 2024-02-07.
- ²¹T. Ishikawa, S. A. Hayes, S. Keskin, G. Corthey, M. Hada, K. Pichugin, A. Marx, J. Hirscht, K. Shionuma, K. Onda, Y. Okimoto, S.-y. Koshihara, T. Yamamoto, H. Cui, M. Nomura, Y. Oshima, M. Abdel-Jawad, R. Kato, and R. J. D. Miller, "Direct observation of collective modes coupled to molecular orbital-driven charge transfer," *Science* **350**, 1501–1505 (2015).
- ²²J. Yang, J. Beck, C. J. Uiterwaal, and M. Centurion, "Imaging of Alignment and Structural Changes of Carbon Disulfide Molecules Using Ultrafast Electron Diffraction," *Nat. Commun.* **6**, 8172 (2015).
- ²³J. Yang, X. Zhu, T. J. Wolf, Z. Li, J. P. F. Nunes, R. Coffee, J. P. Cryan, M. Gühr, K. Hegazy, T. F. Heinz, *et al.*, "Imaging CF₃I conical intersection and photodissociation dynamics with ultrafast electron diffraction," *Science* **361**, 64–67 (2018).
- ²⁴T. J. A. Wolf, D. M. Sanchez, J. Yang, R. M. Parrish, J. P. F. Nunes, M. Centurion, R. Coffee, J. P. Cryan, M. Gühr, K. Hegazy, A. Kirrander, R. K. Li, J. Ruddock, X. Shen, T. Veccione, S. P. Weathersby, P. M. Weber, K. Wilkin, H. Yong, Q. Zheng, X. J. Wang, M. P. Minitti, and T. J. Martínez, "Imaging the photochemical ring-opening of 1,3-cyclohexadiene by ultrafast electron diffraction," *Nat. Chem.* **11**, 504–509 (2019), <https://doi.org/10.1021/acs.jctc.8b01051>.
- ²⁵W. O. Rasmus, K. Acheson, P. Bucksbaum, M. Centurion, E. Champenois, I. Gabalski, M. C. Hoffman, A. Howard, M.-F. Lin, Y. Liu, P. Nunes, S. Saha, X. Shen, M. Ware, E. M. Warne, T. Weinacht, K. Wilkin, J. Yang, T. J. A. Wolf, A. Kirrander, R. S. Minns, and R. Forbes, "Multichannel photodissociation dynamics in CS₂ studied by ultrafast electron diffraction," *Phys. Chem. Chem. Phys.* **24**, 15416–15427 (2022).
- ²⁶M. P. Minitti, J. M. Budarz, A. Kirrander, J. S. Robinson, D. Ratner, T. J. Lane, D. Zhu, J. M. Glowina, M. Kozina, H. T. Lemke, M. Sikorski, Y. Feng, S. Nelson, K. Saita, B. Stankus, T. Northey, J. B. Hastings, and P. M. Weber, "Imaging molecular motion: Femtosecond x-ray scattering of an electrocyclic chemical reaction," *Phys. Rev. Lett.* **114**, 255501 (2015).
- ²⁷J. M. Ruddock, N. Zotev, B. Stankus, H.-W. Yong, D. Bellshaw, S. Boutet, T. J. Lane, M. Liang, S. Carbajo, W. Du, A. Kirrander, M. P. Minitti, and P. M. Weber, "Simplicity beneath complexity: Counting molecular electrons reveals transients and kinetics of photodissociation reactions," *Angew. Chem. Int. Ed.* **58**, 6371–6375 (2019).
- ²⁸J. M. Ruddock, H. Yong, B. Stankus, W. Du, N. Goff, Y. Chang, A. Odate, A. M. Carrascosa, D. Bellshaw, N. Zotev, M. Liang, S. Carbajo, J. Koglin, J. S. Robinson, S. Boutet, A. Kirrander, M. P. Minitti, and P. M. Weber, "A deep uv trigger for ground-state ring-opening dynamics of 1,3-cyclohexadiene," *Sci. Adv.* **5**, eaax6625 (2019).
- ²⁹I. Gabalski, M. Sere, K. Acheson, F. Allum, S. Boutet, G. Dixit, R. Forbes, J. M. Glowina, N. Goff, K. Hegazy, A. J. Howard, M. Liang, M. P. Minitti, R. S. Minns, A. Natan, N. Peard, W. O. Rasmus, R. J. Senson, M. R. Ware, P. M. Weber, N. Werby, T. J. A. Wolf, A. Kirrander, and P. H. Bucksbaum, "Transient vibration and product formation of photoexcited CS₂ measured by time-resolved x-ray scattering," *J. Chem. Phys.* **157**, 164305 (2022).
- ³⁰J. Yang, X. Zhu, J. P. F. Nunes, J. K. Yu, R. M. Parrish, T. J. A. Wolf, M. Centurion, M. Gühr, R. Li, Y. Liu, B. Moore, M. Niebuhr, S. Park, X. Shen, S. Weathersby, T. Weinacht, T. J. Martínez, and X. Wang, "Simultaneous observation of nuclear and electronic dynamics by ultrafast electron diffraction," *Science* **368**, 885–889 (2020).
- ³¹H. Yong, N. Zotev, J. M. Ruddock, B. Stankus, M. Simmermacher, A. M. Carrascosa, W. Du, N. Goff, Y. Chang, D. Bellshaw, M. Liang, S. Carbajo, J. E. Koglin, J. S. Robinson, S. Boutet, M. P. Minitti, A. Kirrander, and P. M. Weber, "Observation of the molecular response to light upon photoexcitation," *Nat. Comm.* **11**, 2157 (2020).
- ³²A. W. Prentice, J. P. Coe, and M. J. Paterson, "Modular Approach to Selected Configuration Interaction in an Arbitrary Spin Basis: Implementation and Comparison of Approaches," *J. Chem. Theory Comp.* **19**, 9161–9176 (2023).
- ³³D. Jacquemin, F. Kossoski, F. Gam, M. Boggio-Pasqua, and P. F. Loos, "Reference Vertical Excitation Energies for Transition Metal Compounds," *Journal of Chemical Theory and Computation* **19**, 8782–8800 (2023), arXiv:2309.17311.
- ³⁴J. E. Runeson and D. E. Manolopoulos, "A multi-state mapping approach to surface hopping," *J. Chem. Phys.* **159**, 094115 (2023).
- ³⁵H.-D. Meyer, U. Manthe, and L. Cederbaum, "The multi-configurational time-dependent Hartree approach," *Chemical Physics Letters* **165**, 73–78 (1990).
- ³⁶M. H. Beck, A. Jäckle, G. A. Worth, and H. D. Meyer, "The multiconfiguration time-dependent Hartree (MCTDH) method: A highly efficient algorithm for propagating wavepackets," *Physics Report* **324**, 1–105 (2000).
- ³⁷F. Wang and T. Ziegler, "The performance of time-dependent density functional theory based on a noncollinear exchange-correlation potential in the calculations of excitation energies," *Journal of Chemical Physics* **122** (2005), 10.1063/1.1844299.
- ³⁸G. A. Worth, M. A. Robb, and I. Burghardt, "A novel algorithm for non-adiabatic direct dynamics using variational Gaussian wavepackets," *Faraday Discussions* **127**, 307 (2004).
- ³⁹B. Lasorne, M. J. Bearpark, M. A. Robb, and G. A. Worth, "Direct quantum dynamics using variational multi-configuration Gaussian wavepackets," *Chemical Physics Letters* **432**, 604–609 (2006).
- ⁴⁰G. Richings, I. Polyak, K. Spinlove, G. Worth, I. Burghardt, and B. Lasorne, "Quantum dynamics simulations using Gaussian wavepackets: the

- vMCG method,” *International Reviews in Physical Chemistry* **34**, 269–308 (2015).
- ⁴¹B. F. E. Curchod and T. J. Martínez, “Ab Initio Nonadiabatic Quantum Molecular Dynamics,” *Chemical Reviews* **118**, 3305–3336 (2018).
- ⁴²T. J. Martínez, M. Ben-Nun, and R. D. Levine, “Molecular Collision Dynamics on Several Electronic States,” *The Journal of Physical Chemistry A* **101**, 6389–6402 (1997).
- ⁴³T. J. Martínez, M. Ben-Nun, and R. D. Levine, “Multi-Electronic-State Molecular Dynamics: A Wave Function Approach with Applications,” *The Journal of Physical Chemistry* **100**, 7884–7895 (1996).
- ⁴⁴T. J. Martínez and R. D. Levine, “Non-adiabatic molecular dynamics: Split-operator multiple spawning with applications to photodissociation,” *Journal of the Chemical Society, Faraday Transactions* **93**, 941–947 (1997).
- ⁴⁵D. V. Shalashilin, “Quantum mechanics with the basis set guided by Ehrenfest trajectories: Theory and application to spin-boson model,” *The Journal of Chemical Physics* **130** (2009), 10.1063/1.3153302.
- ⁴⁶K. Saita and D. V. Shalashilin, “On-the-fly ab initio molecular dynamics with multiconfigurational Ehrenfest method,” *The Journal of Chemical Physics* **137** (2012), 10.1063/1.4734313.
- ⁴⁷D. V. Makhov, C. Symonds, S. Fernandez-Alberti, and D. V. Shalashilin, “Ab initio quantum direct dynamics simulations of ultrafast photochemistry with Multiconfigurational Ehrenfest approach,” *Chem. Phys.* **493**, 200–218 (2017).
- ⁴⁸J. C. Tully, “Molecular dynamics with electronic transitions,” *The Journal of Chemical Physics* **93**, 1061–1071 (1990).
- ⁴⁹H.-D. Meyer and W. H. Miller, “A classical analog for electronic degrees of freedom in nonadiabatic collision processes,” *The Journal of Chemical Physics* **70**, 3214–3223 (1979).
- ⁵⁰S. J. Cotton and W. H. Miller, “Symmetrical Windowing for Quantum States in Quasi-Classical Trajectory Simulations,” *The Journal of Physical Chemistry A* **117**, 7190–7194 (2013).
- ⁵¹W. H. Miller and S. J. Cotton, “Classical molecular dynamics simulation of electronically non-adiabatic processes,” *Faraday Discussions* **195**, 9–30 (2016).
- ⁵²J. E. Runeson and J. O. Richardson, “Generalized spin mapping for quantum-classical dynamics,” *The Journal of Chemical Physics* **152** (2020), 10.1063/1.5143412.
- ⁵³L. González and R. Lindh, eds., *Quantum Chemistry and Dynamics of Excited States: Methods and Applications*, 1st ed. (John Wiley and Sons, United Kingdom, 2021) pp. 1–662.
- ⁵⁴M. Ruckebauer, S. Mai, P. Marquetand, and L. González, “Revealing deactivation pathways hidden in time-resolved photoelectron spectra,” *Sci. Rep.* **6**, 35522 (2016).
- ⁵⁵D. Bellshaw, D. A. Horke, A. D. Smith, H. M. Watts, E. Jager, E. Springate, O. Alexander, C. Cacho, R. T. Chapman, A. Kirrander, and R. S. Minns, “Ab-initio surface hopping and multiphoton ionisation study of the photodissociation dynamics of CS₂,” *Chem. Phys. Lett.* **683**, 383–388 (2017).
- ⁵⁶R. J. Squibb, M. Sapunar, A. Ponzi, R. Richter, A. Kivimäki, O. Plekan, P. Finetti, N. Sisourat, V. Zhaunerchyk, T. Marchenko, L. Journel, R. Guillemin, R. Cucini, M. Coreno, C. Grazioli, M. D. Fraia, C. Callegari, K. C. Prince, P. Decleva, M. Simon, J. H. D. Eland, N. Doslić, R. Feifel, and M. N. Piancastelli, “Acetylacetone Photodynamics at a Seeded Free-Electron Laser,” *Nat. Commun.* **9**, 63 (2018).
- ⁵⁷I. Polyak, L. Hutton, R. Crespo-Otero, M. Barbatti, and P. J. Knowles, “Ultrafast Photoinduced Dynamics of 1,3-Cyclohexadiene Using XMS-CASPT2 Surface Hopping,” *Journal of Chemical Theory and Computation* **15**, 3929–3940 (2019).
- ⁵⁸P. Chakraborty, Y. Liu, T. Weinacht, and S. Matsika, “Excited state dynamics of cis,cis-1,3-cyclooctadiene: Non-adiabatic trajectory surface hopping,” *J. Chem. Phys.* **152**, 174302 (2020).
- ⁵⁹I. C. D. Merritt, D. Jacquemin, and M. Vacher, “cis → trans photoisomerisation of azobenzene: a fresh theoretical look,” *Physical Chemistry Chemical Physics* **23**, 19155–19165 (2021).
- ⁶⁰L. Hutton and B. F. E. Curchod, “Photodynamics of Gas-Phase Pyruvic Acid Following Light Absorption in the Actinic Region,” *ChemPhotoChem* **6** (2022), 10.1002/cptc.202200151.
- ⁶¹K. D. Borne, J. C. Cooper, M. N. R. Ashfold, J. Bachmann, S. Bhattacharyya, R. Boll, M. Bonanomi, M. Bosch, C. Callegari, M. Centurion, M. Coreno, B. F. E. Curchod, M. B. Danailov, A. Demidovich, M. Di Fraia, B. Erk, D. Faccialà, R. Feifel, R. J. G. Forbes, C. S. Hansen, D. M. P. Holland, R. A. Ingle, R. Lindh, L. Ma, H. G. McGhee, S. B. Muvva, J. P. F. Nunes, A. Odate, S. Pathak, O. Plekan, K. C. Prince, P. Rebernik, A. Rouzée, A. Rudenko, A. Simoncig, R. J. Squibb, A. S. Venkatachalam, C. Vozzi, P. M. Weber, A. Kirrander, and D. Rolles, “Ultrafast electronic relaxation pathways of the molecular photoswitch quadricyclane,” *Nature Chem.* (2024), 10.1038/s41557-023-01420-w.
- ⁶²M. Barbatti, “Nonadiabatic dynamics with trajectory surface hopping method,” *WIREs Comput Mol Sci* **1**, 620–633 (2011).
- ⁶³S. Blanes and P. Moan, “Practical symplectic partitioned runge–kutta and runge–kutta–nyström methods,” *Journal of Computational and Applied Mathematics* **142**, 313–330 (2002).
- ⁶⁴R. Crespo-Otero and M. Barbatti, “Recent Advances and Perspectives on Nonadiabatic Mixed Quantum–Classical Dynamics,” *Chemical Reviews* **118**, 7026–7068 (2018).
- ⁶⁵S. Hammes-Schiffer and J. C. Tully, “Proton transfer in solution: Molecular dynamics with quantum transitions,” *The Journal of Chemical Physics* **101**, 4657–4667 (1994).
- ⁶⁶F. Plasser, M. Ruckebauer, S. Mai, M. Oettel, P. Marquetand, and L. González, “Efficient and Flexible Computation of Many-Electron Wave Function Overlaps,” *Journal of Chemical Theory and Computation* **12**, 1207–1219 (2016).
- ⁶⁷G. Granucci, M. Persico, and A. Zocante, “Including quantum decoherence in surface hopping,” *The Journal of Chemical Physics* **133** (2010), 10.1063/1.3489004.
- ⁶⁸J. E. Subotnik, A. Jain, B. Landry, A. Petit, W. Ouyang, and N. Bellonzi, “Understanding the Surface Hopping View of Electronic Transitions and Decoherence,” *Ann. Rev. Phys. Chem.* **67**, 387–417 (2016).
- ⁶⁹J. R. Mannouch and J. O. Richardson, “A mapping approach to surface hopping,” *The Journal of Chemical Physics* **158** (2023), 10.1063/5.0139734.
- ⁷⁰J. E. Runeson, T. P. Fay, and D. E. Manolopoulos, “Exciton dynamics from the mapping approach to surface hopping: comparison with Förster and Redfield theories,” *Physical Chemistry Chemical Physics* (2024), 10.1039/D3CP05926J.
- ⁷¹P. Debye, *Physikalische Zeitschrift* **31**, 419–428 (1930).
- ⁷²L. Bewilogua, *Physikalische Zeitschrift* **33**, 688–692 (1932).
- ⁷³A. Kirrander and P. M. Weber, “Fundamental Limits on Spatial Resolution in Ultrafast X-ray Diffraction,” *Appl. Science* **7**, 534 (2017).
- ⁷⁴M. Simmermacher, P. M. Weber, and A. Kirrander, “Theory of time-dependent scattering,” in *Structural Dynamics with X-ray and Electron Scattering*, Theoretical and Computational Chemistry Series, Vol. 25, edited by K. Amini, A. Rouzée, and M. J. J. Vrakking (Royal Society of Chemistry, United Kingdom, 23 December 2023) 1st ed., Chap. 3, p. 85, www.rsc.org.
- ⁷⁵E. Prince, ed., *International Tables for Crystallography Volume C: Mathematical, physical and chemical tables*, 2006th ed., ISBN 978-1-4020-1900-5 (Wiley, 2006).
- ⁷⁶M. Simmermacher, A. Kirrander, and N. E. Henriksen, “Time-resolved x-ray scattering from impulsively aligned or oriented molecules,” *Phys. Rev. A* **102**, 052825 (2020).
- ⁷⁷F. Salvat, A. Jablonski, and C. J. Powell, “elsepa—Dirac partial-wave calculation of elastic scattering of electrons and positrons by atoms, positive ions and molecules,” *Comp. Phys. Commun.* **165**, 157–190 (2005).
- ⁷⁸A. M. Carrascosa, H. Yong, D. L. Crittenden, P. M. Weber, and A. Kirrander, “Ab-initio calculation of total x-ray scattering from molecules,” *J. Chem. Theory Comp.* **15**, 2836–2846 (2019), <https://doi.org/10.1021/acs.jctc.9b00056>.
- ⁷⁹N. Zotev, A. M. Carrascosa, M. Simmermacher, and A. Kirrander, “Excited Electronic States in Total Isotropic Scattering from Molecules,” *J. Chem. Theory Comput.* **16**, 2594–2605 (2020).
- ⁸⁰A. M. Carrascosa, J. P. Coe, M. Simmermacher, M. J. Paterson, and A. Kirrander, “Towards high-resolution X-ray scattering as a probe of electron correlation,” *Phys. Chem. Chem. Phys.* **24**, 24542–24552 (2022).
- ⁸¹B. O. Roos, P. R. Taylor, and P. E. Sigbahn, “A complete active space SCF method (CASSCF) using a density matrix formulated super-CI approach,” *Chemical Physics* **48**, 157–173 (1980).
- ⁸²D. E. Woon and T. H. Dunning, “Gaussian basis sets for use in correlated molecular calculations. III. The atoms aluminum through argon,” *The Journal of Chemical Physics* **98**, 1358–1371 (1993).
- ⁸³F. Aquilante, J. Autschbach, A. Baiardi, S. Battaglia, V. A. Borin, L. F. Chibotaru, I. Conti, L. De Vico, M. Delcey, I. Fdez. Galván, N. Ferré, L. Fre-

- itag, M. Garavelli, X. Gong, S. Knecht, E. D. Larsson, R. Lindh, M. Lundberg, P. Å. Malmqvist, A. Nenov, J. Norell, M. Odellius, M. Olivucci, T. B. Pedersen, L. Pedraza-González, Q. M. Phung, K. Pierloot, M. Reiher, I. Schapiro, J. Segarra-Martí, F. Segatta, L. Seijo, S. Sen, D.-C. Sergentu, C. J. Stein, L. Ungur, M. Vacher, A. Valentini, and V. Veryazov, "Modern quantum chemistry with [Open]Molcas," *The Journal of Chemical Physics* **152** (2020), 10.1063/5.0004835.
- ⁸⁴G. Li Manni, I. Fdez. Galván, A. Alavi, F. Aleotti, F. Aquilante, J. Autschbach, D. Avagliano, A. Baiardi, J. J. Bao, S. Battaglia, L. Birnoschi, A. Blanco-González, S. I. Bokarev, R. Broer, R. Cacciari, P. B. Calio, R. K. Carlson, R. Carvalho Couto, L. Cerdán, L. F. Chibotaru, N. F. Chilton, J. R. Church, I. Conti, S. Coriani, J. Cuéllar-Zuquin, R. E. Daoud, N. Dattani, P. Decleva, C. de Graaf, M. G. Delcey, L. De Vico, W. Dobrautz, S. S. Dong, R. Feng, N. Ferré, M. Filatov(Gulak), L. Gagliardi, M. Garavelli, L. González, Y. Guan, M. Guo, M. R. Hennefarth, M. R. Hermes, C. E. Hoyer, M. Huix-Rotllant, V. K. Jaiswal, A. Kaiser, D. S. Kaliakin, M. Khamesian, D. S. King, V. Kochetov, M. Krośnicki, A. A. Kumar, E. D. Larsson, S. Lehtola, M.-B. Lepetit, H. Lischka, P. López Ríos, M. Lundberg, D. Ma, S. Mai, P. Marquetand, I. C. D. Merritt, F. Montorsi, M. Mörchen, A. Nenov, V. H. A. Nguyen, Y. Nishimoto, M. S. Oakley, M. Olivucci, M. Oppel, D. Padula, R. Pandharkar, Q. M. Phung, F. Plasser, G. Raggi, E. Rebolini, M. Reiher, I. Rivalta, D. Roca-Sanjuán, T. Romig, A. A. Safari, A. Sánchez-Mansilla, A. M. Sand, I. Schapiro, T. R. Scott, J. Segarra-Martí, F. Segatta, D.-C. Sergentu, P. Sharma, R. Shepard, Y. Shu, J. K. Staab, T. P. Straatsma, L. K. Sørensen, B. N. C. Tenorio, D. G. Truhlar, L. Ungur, M. Vacher, V. Veryazov, T. A. Voß, O. Weser, D. Wu, X. Yang, D. Yarkony, C. Zhou, J. P. Zobel, and R. Lindh, "The OpenMolcas Web : A Community-Driven Approach to Advancing Computational Chemistry," *Journal of Chemical Theory and Computation* **19**, 6933–6991 (2023).
- ⁸⁵T. Shiozaki, W. Győrffy, P. Celani, and H.-J. Werner, "Communication: Extended multi-state complete active space second-order perturbation theory: Energy and nuclear gradients," *The Journal of Chemical Physics* **135** (2011), 10.1063/1.3633329.
- ⁸⁶N. Forsberg and P.-Å. Malmqvist, "Multiconfiguration perturbation theory with imaginary level shift," *Chemical Physics Letters* **274**, 196–204 (1997).
- ⁸⁷J. B. Schriber and F. A. Evangelista, "Communication: An adaptive configuration interaction approach for strongly correlated electrons with tunable accuracy," *The Journal of Chemical Physics* **144** (2016), 10.1063/1.4948308.
- ⁸⁸J. B. Schriber and F. A. Evangelista, "Adaptive Configuration Interaction for Computing Challenging Electronic Excited States with Tunable Accuracy," *Journal of Chemical Theory and Computation* **13**, 5354–5366 (2017).
- ⁸⁹A. W. Prentice, J. P. Coe, and M. J. Paterson, "Modular Approach to Selected Configuration Interaction in an Arbitrary Spin Basis: Implementation and Comparison of Approaches," *Journal of Chemical Theory and Computation* **19**, 9161–9176 (2023).
- ⁹⁰L. Tong, M. Nolan, T. Cheng, and J. Greer, "A Monte Carlo configuration generation computer program for the calculation of electronic states of atoms, molecules, and quantum dots," *Computer Physics Communications* **131**, 142–163 (2000).
- ⁹¹J. P. Coe and M. J. Paterson, "State-averaged Monte Carlo configuration interaction applied to electronically excited states," *The Journal of Chemical Physics* **139** (2013), 10.1063/1.4824888.
- ⁹²A. Prentice, J. Coe, and M. Paterson, "Generalsci 1.0," (2023), <https://doi.org/10.5281/zenodo.10203394>.
- ⁹³R. Crespo-Otero and M. Barbatti, "Spectrum simulation and decomposition with nuclear ensemble: formal derivation and application to benzene, furan and 2-phenylfuran," *Theoretical Chemistry Accounts* **131**, 1237 (2012).
- ⁹⁴S. Mai, P. Marquetand, and L. González, "Nonadiabatic dynamics: The SHARC approach," *WIREs Computational Molecular Science* **8** (2018), 10.1002/wcms.1370.
- ⁹⁵A. Udvarhazi and M. A. El-Sayed, "Vacuum-Ultraviolet Spectra of Cyclic Ketones," *The Journal of Chemical Physics* **42**, 3335–3336 (1965).
- ⁹⁶I. Fdez. Galván, M. G. Delcey, T. B. Pedersen, F. Aquilante, and R. Lindh, "Analytical State-Average Complete-Active-Space Self-Consistent Field Nonadiabatic Coupling Vectors: Implementation with Density-Fitted Two-Electron Integrals and Application to Conical Intersections," *Journal of Chemical Theory and Computation* **12**, 3636–3653 (2016).